Influence of the polymer properties and numerical schemes on tertiary oil recovery processes

Druetta, P.; Picchioni, F.

Published in:
Computers & Mathematics with Applications

DOI:
10.1016/j.camwa.2019.08.028

Computers and Mathematics with Applications 79 (2020) 1094–1110

Contents lists available at ScienceDirect

Computers and Mathematics with Applications

journal homepage: www.elsevier.com/locate/camwa

Influence of the polymer properties and numerical schemes on tertiary oil recovery processes

P. Druetta, F. Picchioni *

Department of Chemical Engineering, ENTEG, University of Groningen, Nijenborgh 4, 9747AG, Groningen, The Netherlands

ARTICLE INFO

Article history:
Received 20 September 2018
Accepted 24 August 2019
Available online 25 September 2019

Keywords:
EOR
Polymer
Degradation
Viscoelasticity
Reservoir simulation
TVD

ABSTRACT

Chemical Enhanced Oil Recovery (EOR) processes comprise a number of flooding techniques aimed at increasing the operational life of mature oilfields. Among these, polymer flooding is one of the most developed; its functionality is to increment the aqueous viscosity, avoiding the formation of viscous fingering. Reservoir simulators consider this influence as well as other physical properties (e.g., adsorption, permeability reduction). However, the polymer degradation is usually not considered even though it plays a critical role in the viscosity. In this paper this mechanism is analyzed and coupled with the previously mentioned physical phenomena in order to present a complete study of their influence in the EOR process. Moreover, since a fully second-order accuracy scheme is used along with a Total Variation Diminishing (TVD) flux-limiting function, the influence of the latter on the recovery factor is also discussed. Results showed that the negative effect of the polymer adsorption was the most relevant physical phenomenon in terms of the oil recovery. Furthermore, the analysis of the discretization of the differential equations showed that traditional, linear first-order schemes created numerical diffusion affecting negatively the macroscopic sweeping efficiency, which disappeared when TVD techniques were used. Reservoir simulators allow determining the desired designing properties for future polymers in relationship with the characteristics of the oilfield to be exploited.

1. Introduction

Since the beginning of the industrial revolution almost 200 years ago, several energy sources were employed for the steadily increasing demand of the society and industrial processes. These sources are mostly of organic or fossil origin, affecting the environment. In addition, due to the relationship between the rate of use of these fuels and their speed of formation, humanity has turned them into non-renewable resources. Therefore, during the last years the trend has been to develop new sources of energy, renewable and “greener”, in order to replace fossil hydrocarbons. However, current technology makes it not feasible for them to replace those derived from oil, gas, wood and coal, although they now account for 20% of the total world consumption. Given this situation, and the strong dependence of the world economy on these sources, the possibilities are in this context reduced to: finding new sources of fossil resources, or extending the operational life and performance of fields already mature, close to or above the economic limit of exploitation. Enhanced Oil Recovery focuses on the latter, developing different processes according to the physical properties of the rock formation and oil trapped in it [1,2].

* Corresponding author.
E-mail address: f.picchioni@rug.nl (F. Picchioni).
URL: http://www.rug.nl/research/product-technology/ (F. Picchioni).

https://doi.org/10.1016/j.camwa.2019.08.028
0898-1221/

Nomenclature

Cr	Courant Number
$\underline{\underline{D}}$	Dispersion Tensor
dm	Molecular Diffusion [m^2/s]
dl	Longitudinal Dispersion [m^2/s]
dt	Transversal Dispersion [m^2/s]
F_{LIM}	Flux Limiter Function
k_r	Relative Permeability
p	Reservoir Pressure [Pa]
p_{wf}	Bottomhole Pressure [Pa]
r	Volumetric Concentration Gradient
r_w	Well Radius [m]
S	Phase Saturation
s	Well Skin Factor
V	Volumetric Concentration
z	Overall Concentration

Greek Letters

Γ	Domain Boundary
δ_{ij}	Kronecker Delta
λ	Phase Mobility [$m^2/(Pa \cdot s)$]
μ	Absolute Viscosity [$Pa \cdot s$]
σ	Interfacial Tension [mN/m]
Ω	Reservoir Domain

Superscripts

a	Aqueous Phase
H	Water–Oil System (no Chemical)
j	Phase
$[k]$	Iteration Number
$\langle n \rangle$	Time-Step
o	Oleous Phase
r	Residual

Subscripts

c	Chemical Component
i	Component
in	Injection
m, n	Spatial Grid Blocks
p	Petroleum Component
t	Total
w	Water Component

1.1. Previous numerical research

Many articles and reports have been published dealing with the modeling of non-Newtonian and viscoelastic fluids in porous media, describing the mathematical models used in most non-Newtonian fluids, as well as the most commonly used formulations to describe the extra-stress tensor in viscoelastic materials [3–5]. It can be considered that there are two main streams in the literature to model the effects of viscoelasticity. The first method is to follow the traditional route and to model the effects such as the phenomenon of "shear-thickening" occurring at high shear rates, which is also called elongational viscosity. While this phenomenon actually occurs in reality, these combined models of shear-thinning and shear-thickening lack of the extra stress tensor, which calculates the normal stresses arising within the fluid. The second approach is to model this extra stress tensor following some of the correlations already used and known (e.g., UCM, Oldroyd-B), which lack of the shear-thinning phenomena observed during rheological tests.

Under the first one, which is the typical approach in reservoir simulation, one of the latest results produced was made by Cao [6], who developed a mathematical model of viscoelastic polymer flooding for EOR. The model combined a "viscoelastic" constitutive model which consisted in a shear-thickening rheology behavior, using this to model the residual oil saturation reduction related to polymer's viscoelasticity. To solve the system, an implicit operator splitting method was used, along with a Total Variation Diminishing to handle the upwind scheme. The results showed that the pressure gradient will increase caused by the viscoelasticity of polymer, and the elastic behavior plays the important role under high flow velocity. Zamani [7] studied a model solving the Navier–Stokes equations for non-Newtonian fluids in three- (using real rock images) and two-dimensions (simplified pore geometries), using the finite-difference method. He observed that, when a higher degree of shear thickening is induced, more flow diversion to side channels perpendicular to the main flow path and larger drag on fluids inside side channels will occur, which is consistent with experimental findings. Furthermore, Kamyabi [8,9] performed numerical simulations of Carreau and Power-Law fluids flow in an open capillary connected to a "dead-end" using finite volume methods (FVM). The effects of fluids, the operating conditions and the aspect ratio of "dead-end" on the oil recovery factor were also investigated. The simulation showed that increasing the Power-Law exponent (i.e., shear thinning region) was favorable to the oil recovery in the "dead-end". On the other hand, the effect of the Reynolds number was insignificant at the investigated conditions. Zheng [10] studied a viscoelastic polymer solution with a transient network structure due to the entanglement of molecules, flowing through porous media. Then he performed a 3D viscoelastic polymer flooding model to examine the effect of elasticity on the EOR process. The results demonstrated that the oil recovery of viscoelastic polymer flooding can be enhanced by larger displacement efficiency due to its microscopic roles. Relaxation time, as a major characteristic parameter of viscoelastic polymer, plays a decisive role. When the polymer solutions flow through the porous media, shear flow and elongational flow coexist. He modeled the effect of shear thickening as a composition of shear and elastic viscosities, just as modeled by Delshad [11]. Finally, Wang [12] based on the theory and application developments of polymer flooding on enhancing oil recovery, developed an improved mathematical model to simulate the mechanism of viscoelastic polymer flooding. The IMPES method was used in this case to solve the flooding model considering the viscosifying effect on elasticity, decreasing residual oil as well as the degradation of polymer molecules.

2. Aim of this work

The aim of this paper consists in extending the work performed with polymer EOR simulators, developing a fully second-order system with TVD flux limiting functions in order to solve the differential equations of the compositional model, valid in chemical tertiary recovery processes. This, along with a novel physical description of polymer properties, including phenomena not considered before by previous simulators, rendered a novel system which considers as well the polymer degradation and the viscoelastic properties. The latter are considered both in the shear-thickening rheology behavior and in the effect of the normal, viscoelastic stresses on the residual oil saturation.

This paper is focused on studying firstly the influence of the numerical schemes on the recovery factors. It is well known that first order, linear schemes produce artificial diffusion of the different components which, in the case of the polymer, provokes a smearing of the chemical slug, decreasing the viscosity and thus the efficiency. Non-linear TVD schemes with flux limiting functions are proposed as a mean of decreasing this undesired phenomena and allow a better tracking of the chemical front, without the appearance of spurious oscillations [13]. The second part of this study consists in studying the influence of the diffusion and adsorption in the recovery processes with polymers. Both phenomena have a negative effect on the recovery process, with the adsorption being considered one of the main problems in EOR. These, coupled with the novel degradation and rheology models, allowed studying the behavior of the chemical in the oil field from a new perspective. The combination of the mentioned has resulted in a novel and complete simulator, which can be used for the design and screening of new polymers to be used in EOR.

2.1. Physical model

In order to model the EOR process in a 2D oil field a specific geometric well pattern is used, usually found in the oil industry. The five-spot scheme is one of the standard configurations, consisting of a square domain in which an injection well is placed at the center and four producing wells at the corners. A simplification of this is the quarter of five-spot, which is commonly used in reservoir simulation and academic research (Fig. 1). The physical model is composed by a reservoir (Ω) of known geometric characteristics, with an absolute permeability (K) and porosity (ϕ), which can be considered constants or to have a statistical distribution. The flow is considered isothermal, incompressible and 2-dimensional (since it is assumed that the vertical permeability is negligible when compared to horizontal ones). The domain is then discretized in a system of $n_x \times n_y$ blocks to perform the numerical simulation. The Darcy's law is valid and gravitational forces are negligible compared to the viscous ones [14].

Chemical polymer EOR flooding consists in the injection of an aqueous solution with the polymer, followed by a water bank in order to drive the chemical plug, sweeping the mobilized oil into the producing wells. This model is represented by a system of strongly non-linear parabolic/elliptic partial differential equations (PDE), complemented by a set of algebraic relationships representing physical properties of the fluid and the rock, namely: interfacial tension, residual phase saturations, relative permeabilities, rock wettability, disproportionate permeability reduction, inaccessible pore volume, chemical degradation, viscoelastic properties, phase viscosities, capillary pressure, adsorption, and dispersion [1,2,15].

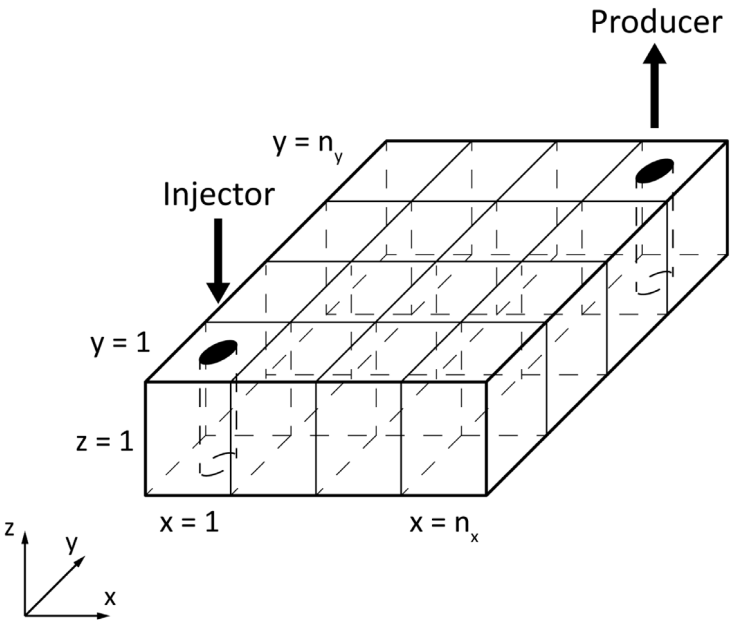

Fig. 1. Schematic representation of the quarter 5-spot used for the EOR simulations.

2.2. Mathematical model

In the case of chemical EOR, the phases and rock's properties depend, to a greater or lesser extent, on the concentration of the components, rendering a strongly non-linear system in which traditional reservoir simulation schemes (e.g., black-oil) are not suitable. The compositional flow, on the other hand, allows the simulation of multiphase, multicomponent systems in which the properties are expressed as functions of the components' concentrations. The numerical simulator presented in this paper is based on a previous one developed also for EOR flooding [16], which was validated against commercial and academic simulators in 2D flooding processes (Fig. 2). Since this model it is an extension of a previous one, already validated, it is considered in this study that the validation process previously done is valid for this model [17–19]. Thus, the Darcy, mass conservation (along with the dispersion tensor) and aqueous pressure equations describing the system are,

$$\vec{u}^j = -\underline{\underline{K}} \cdot \frac{k_r^j}{\mu^j} \cdot \vec{\nabla} p^j \quad ; \quad j = o, a \tag{1}$$

$$\frac{\partial (\phi z_i)}{\partial t} + \nabla \cdot \sum_j V_i^j \cdot \vec{u}^j - \nabla \cdot \sum_j \underline{\underline{D}}_i^j \cdot \nabla \cdot V_i^j = -\frac{\partial (\phi A d_i)}{\partial t} + q_i \quad ; \quad i = p, c, w \tag{2}$$

$$\underline{\underline{D}}_i^j = dm_i^j \cdot \phi \cdot S^j \cdot \delta_{ij} + \|\vec{u}^j\| \cdot \left[\frac{d l^j}{\|\vec{u}^j\|^2} \cdot \begin{pmatrix} (u_x^j)^2 & u_x^j \cdot u_y^j \\ u_y^j \cdot u_x^j & (u_y^j)^2 \end{pmatrix} + dt^j \cdot \begin{pmatrix} 1 - \frac{(u_x^j)^2}{\|\vec{u}^j\|^2} & -\frac{u_x^j \cdot u_y^j}{\|\vec{u}^j\|^2} \\ -\frac{u_y^j \cdot u_x^j}{\|\vec{u}^j\|^2} & 1 - \frac{(u_y^j)^2}{\|\vec{u}^j\|^2} \end{pmatrix} \right] \tag{3}$$

$$\phi c_r \frac{\partial p^a}{\partial t} + \vec{\nabla} \cdot (\lambda \cdot \nabla p^a) = \frac{\partial}{\partial t} \left(\phi \cdot \sum_i A d_i \right) - \vec{\nabla} \cdot \left(\lambda^o \cdot \nabla p_c \right) + q_t \tag{4}$$

The diffusive flux it is caused by several sources with the simplest movement one being is molecular diffusion described by the random Brownian motion of molecules. Usually in reservoir simulations the latter is negligible when compared to other considered forces acting on the fluids. But also mechanical dispersion is present. Narrow channel flows experience parabolic diffusion along the fronts (Taylor dispersion) and the irregular pore networks disperse the mass at a microscale. Besides this, the phenomena of transverse and longitudinal (tortuosity effect) spreading are also present.

As it was mentioned previously, the main functionality of the polymer is to increase the viscosity of the displacing phase, reducing the mobility ratio, and avoiding the formation of viscous fingering in the reservoir. [22–25] Along

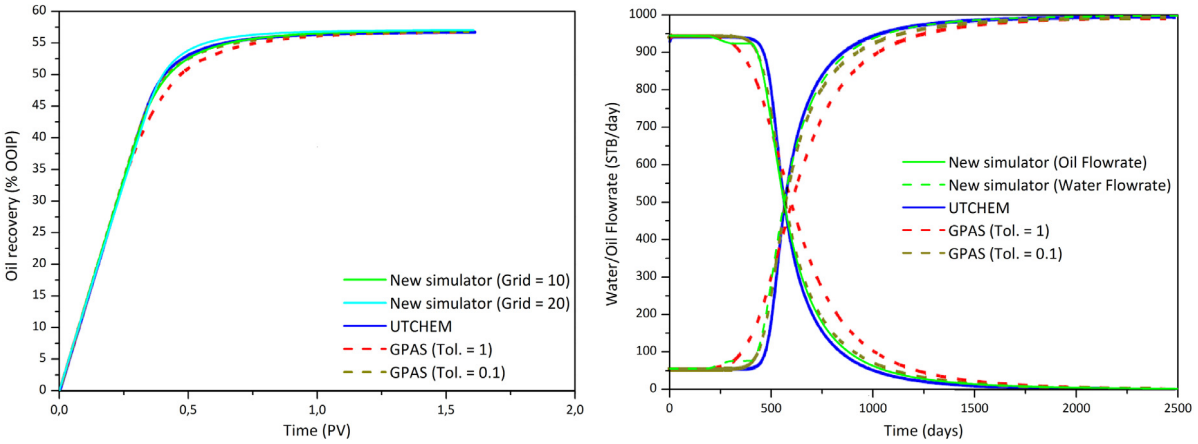

Fig. 2. Oil recovery factor (left) and flowrates (in Standard Barrels per day — right) during a waterflooding and comparison with the results obtained with UTCHEM and GPAS.
Source: Adapted from Najafabadi [20] and Druetta [21].

with this, it is also studied in this paper the influence of several well-known phenomena in the process, such as the physical diffusion of the polymer in the aqueous phase, and the adsorption of the polymer molecules onto the rock formation. These are well-documented aspects of polymer flooding, which have already been taken into account in previous simulators. [6,20,26–32]

This renders a system of non-linear parabolic partial differential equations, which is discretized by a finite difference method. The pressure of the aqueous phase (Eq. (4)) is implicitly solved using a centered scheme for the pressure terms and a second-order Taylor approximation in the time derivatives. Furthermore, the total and aqueous Darcy velocities are also presented and explicitly solved using the same centered scheme. Therefore, Eqs. (4) and (1) are discretized as,

$$
\begin{aligned}
&c_r\left(\phi+\tfrac{\Delta t}{2}\tfrac{\partial\phi}{\partial t}\right)^{\langle n+1\rangle,[k]}_{m,n}\left(\frac{p^{a,\langle n+1\rangle}_{m,n}-p^{a,\langle n\rangle}_{m,n}}{\Delta t}\right)^{[k+1]}+\frac{\lambda^{\langle n+1\rangle,[k]}_{x,m+1/2,n}}{\Delta x^2}\cdot\left(p^a_{m+1,n}-p^a_{m,n}\right)^{\langle n+1\rangle,[k+1]}-\cdots\\
&-\frac{\lambda^{\langle n+1\rangle,[k]}_{x,m-1/2,n}}{\Delta x^2}\cdot\left(p^a_{m,n}-p^a_{m-1,n}\right)^{\langle n+1\rangle,[k+1]}+\frac{\lambda^{\langle n+1\rangle,[k]}_{y,m+1/2,n}}{\Delta y^2}\cdot\left(p^a_{m,n+1}-p^a_{m,n}\right)^{\langle n+1\rangle,[k+1]}-\cdots\\
&-\frac{\lambda^{\langle n+1\rangle,[k]}_{y,m-1/2,n}}{\Delta y^2}\cdot\left(p^a_{m,n}-p^a_{m,n-1}\right)^{\langle n+1\rangle,[k+1]}=\left(\phi+\tfrac{\Delta t}{2}\tfrac{\partial\phi}{\partial t}\right)^{\langle n+1\rangle,[k]}_{m,n}\left(\frac{Ad^{\langle n+1\rangle}_{m,n}-Ad^{\langle n\rangle}_{m,n}}{\Delta t}\right)^{[k+1]}+\cdots\\
&+\left(Ad+\tfrac{\Delta t}{2}\tfrac{\partial Ad}{\partial t}\right)^{\langle n+1\rangle,[k]}_{m,n}\left(\frac{\phi^{\langle n+1\rangle}_{m,n}-\phi^{\langle n\rangle}_{m,n}}{\Delta t}\right)^{[k+1]}+\frac{\lambda^{o,\langle n+1\rangle,[k]}_{x,m+1/2,n}}{\Delta x^2}\cdot\left(p^c_{m+1,n}-p^c_{m,n}\right)^{\langle n+1\rangle,[k+1]}-\cdots\\
&-\frac{\lambda^{o,\langle n+1\rangle,[k]}_{x,m-1/2,n}}{\Delta x^2}\cdot\left(p^c_{m,n}-p^c_{m-1,n}\right)^{\langle n+1\rangle,[k+1]}+\frac{\lambda^{o,\langle n+1\rangle,[k]}_{y,m+1/2,n}}{\Delta y^2}\cdot\left(p^c_{m,n+1}-p^c_{m,n}\right)^{\langle n+1\rangle,[k+1]}-\cdots\\
&-\frac{\lambda^{o,\langle n+1\rangle,[k]}_{y,m-1/2,n}}{\Delta y^2}\cdot\left(p^c_{m,n}-p^c_{m,n-1}\right)^{\langle n+1\rangle,[k+1]}+q^{t,\langle n+1\rangle,[k]}_{m,n}
\end{aligned}
\tag{5}
$$

$$
\begin{aligned}
\vec{u}^{\langle n+1\rangle,[k+1]}_{m,n}=&\left[-\frac{\lambda^{[k]}_{x,m,n}}{2\cdot\Delta x}\cdot\left(p^a_{m+1,n}-p^a_{m-1,n}\right)^{[k+1]}-\cdots\right.\\
&\left.-\frac{\lambda^{o,[k]}_{x,m,n}}{2\cdot\Delta x}\cdot\left(p^a_{c,m+1,n}-p^a_{c,m-1,n}\right)^{[k+1]}\right]^{\langle n+1\rangle}\cdot\hat{i}+\left[-\frac{\lambda^{[k]}_{y,m,n}}{2\cdot\Delta y}\cdot\left(p^a_{m,n+1}-p^a_{m,n-1}\right)^{[k+1]}-\cdots\right.\\
&\left.-\frac{\lambda^{o,[k]}_{y,m,n}}{2\cdot\Delta y}\cdot\left(p^a_{c,m,n+1}-p^a_{c,m,n-1}\right)^{[k+1]}\right]^{\langle n+1\rangle}\cdot\hat{j}
\end{aligned}
\tag{6}
$$

$$
\begin{aligned}
\vec{u}^{a,\langle n+1\rangle,[k+1]}_{m,n}=&\left[-\frac{\lambda^{a,[k]}_{x,m,n}}{2\cdot\Delta x}\cdot\left(p^a_{m+1,n}-p^a_{m-1,n}\right)^{[k+1]}\right]^{\langle n+1\rangle}\cdot\hat{i}+\cdots\\
&+\left[-\frac{\lambda^{a,[k]}_{y,m,n}}{2\cdot\Delta y}\cdot\left(p^a_{m,n+1}-p^a_{m,n-1}\right)^{[k+1]}\right]^{\langle n+1\rangle}\cdot\hat{j}
\end{aligned}
\tag{7}
$$

In these equations m, n represent the cells of the physical numerical domain $(x, y) = (m \cdot \Delta x, n \cdot \Delta y)$, respectively, $\langle n\rangle$ represents the temporal-step (time $= \langle n\rangle \cdot \Delta t$) in the simulation and finally $[k]$, $\forall k \in \mathbb{N}^+$, is the iteration number within

Table 1
Most commonly used flux limiter functions [13].

Type	Flux limiter function
Upwind	0
Superbee	$\max[0, \min(2r, 1), \min(r, 2)]$
Minmod	$\max[0, \min(r, 1)]$
MUSCL	$\max\left[0, \min\left(2r, \frac{1+r}{2}, 2\right)\right]$

each time-step. In this system it is of the utmost importance to calculate properly the in- and outflows in the well blocks. In order to do so generally *well models* are used [33]. In this paper it was adopted, in Cartesian coordinates, the following formula:

$$Q = \left[PI_{m,n}^{j,[k]} \cdot \left(p_{wf} - p_{m,n}^{j,[k+1]}\right)\right]^{\langle n+1\rangle} \tag{8}$$

where the productivity ratio $PI_{m,n}^{j,[k]}$ is calculated according to,

$$PI_{m,n}^{j,[k]} = \frac{2 \cdot \pi \cdot \sqrt{k_x \cdot k_y} \cdot \Delta z}{0.15802 \cdot \left[\ln\left(\frac{r_o}{r_w}\right) + s\right]} \cdot \frac{k_r^j}{\mu_{m,n}^j} \tag{9}$$

The equivalent radius r_o is obtained with the Peaceman model for heterogeneous permeability models [33],

$$r_o = 0.28 \cdot \frac{\left[\left(\frac{k_x}{k_y}\right)^{1/2} \cdot \Delta y^2 + \left(\frac{k_y}{k_x}\right)^{1/2} \cdot \Delta x^2\right]^{1/2}}{\left(\frac{k_x}{k_y}\right)^{1/4} + \left(\frac{k_y}{k_x}\right)^{1/4}} \tag{10}$$

Finally, the discretization of the mass conservation equation is analyzed using a second-order approach. Eq. (2) is the typical advection–diffusion PDE, employed in many phenomena in porous media. Advective terms are of hyperbolic nature, and first-order upwind schemes cause a numerical diffusion in the solution [34,35]. In order to diminish the effects of the truncation errors, a fully second-order is proposed in this paper in time and space, based on TVD flux limiters (using a splitting technique). The latter allow a proper tracking of the chemical agent front wave as well as they decrease the occurrence of numerical diffusion and spurious oscillations. On the other hand, the diffusive terms are discretized using a centered second order scheme [36].

A functional relationship is required between the gradient of the volumetric concentration and the limiting function. Several second order methods have been proposed in the literature [13]. The functions used in this simulator are presented in Table 1, along with the standard Upwind method. These functions depend on the ratio of the concentrations' consecutive gradients in the numerical mesh $\left(r_{x,i} = \left(V_{i,m,n}^{j,[k]} - V_{i,m-1,n}^{j,[k]}\right) / \left(V_{i,m+1,n}^{j,[k]} - V_{i,m,n}^{j,[k]}\right)\right)$.

Thus, the discretized mass conservation equation is obtained.

$$\begin{aligned}
\frac{\mathcal{C}_1}{\Delta t} z_i^{\langle n+1\rangle} &= \mathcal{C}_2 z_i^{\langle n\rangle} + \frac{\mathcal{C}_3}{\Delta x} \cdot \sum_j F_{LIM,x}^{j,\langle n+1\rangle,[k+1]} \left(u_{x,m,n}^{j,[k+1]} \cdot V_{i,m,n}^{j,[k]} - u_{x,m-1,n}^{j,[k+1]} \cdot V_{i,m-1,n}^{j,[k]}\right)^{\langle n+1\rangle} + \cdots \\
&+ \frac{\mathcal{C}_3}{\Delta y} \cdot \sum_j F_{LIM,y}^{j,\langle n+1\rangle,[k+1]} \left(u_{y,m,n}^{j,[k+1]} \cdot V_{i,m,n}^{j,[k]} - u_{y,m,n-1}^{j,[k+1]} \cdot V_{i,m,n-1}^{j,[k]}\right)^{\langle n+1\rangle} + \cdots \\
&+ \frac{1}{\Delta x^2} \cdot \sum_j \left[\left(S^j \phi dm_i^j\right)_{m+1/2,n} \cdot \left(V_{i,m+1,n}^j - V_{i,m,n}^j\right) - \left(S^j \phi dm_i^j\right)_{m-1/2,n} \cdot \left(V_{i,m,n}^j - V_{i,m-1,n}^j\right)\right]^{\langle n+1\rangle,[k]} + \cdots \\
&+ \frac{1}{\Delta y^2} \cdot \sum_j \left[\left(S^j \phi dm_i^j\right)_{m,n+1/2} \cdot \left(V_{i,m,n+1}^j - V_{i,m,n}^j\right) - \left(S^j \phi dm_i^j\right)_{m,n-1/2} \cdot \left(V_{i,m,n}^j - V_{i,m,n-1}^j\right)\right]^{\langle n+1\rangle,[k]} - \cdots \\
&- \frac{1}{\Delta t} \left(\phi + \Delta t \frac{\partial \phi}{\partial t}\right)_{m,n}^{\langle n+1\rangle,[k+1]} \cdot \left(Ad_i^{\langle n+1\rangle} - Ad_i^{\langle n\rangle}\right)_{m,n}^{[k]} - \frac{Ad_{i,m,n}^{\langle n+1\rangle,[k]}}{\Delta t} \cdot \left(\phi^{\langle n+1\rangle} - \phi^{\langle n\rangle}\right)_{m,n}^{[k]} + \cdots \\
&+ q_{i,m,n}^{\langle n+1\rangle,[k+1]} + \sum_j \frac{u_{x,m,n}^{j,[k+1]} \Delta t}{2\phi_{m,n}^{\langle n+1\rangle,[k+1]}} \cdot \left(\frac{\partial Ad}{\partial x} \frac{\partial \phi}{\partial t} + Ad \frac{\partial^2 \phi}{\partial t \partial x} + \frac{\partial \phi}{\partial x} \frac{\partial Ad}{\partial t}\right)_{i,m,n}^{\langle n+1\rangle,[k]} + \cdots \\
&+ \sum_j \frac{u_{y,m,n}^{j,[k+1]} \Delta t}{2\phi_{m,n}^{\langle n+1\rangle,[k+1]}} \cdot \left(\frac{\partial Ad}{\partial y} \frac{\partial \phi}{\partial t} + Ad \frac{\partial^2 \phi}{\partial t \partial y} + \frac{\partial \phi}{\partial y} \frac{\partial Ad}{\partial t}\right)_{i,m,n}^{\langle n+1\rangle,[k]} - \cdots \\
&- \sum_j \left(\frac{u_{x,m,n}^{j,[k+1]} \Delta t}{2} \frac{\partial^2 Ad}{\partial t \partial x} + \frac{u_{y,m,n}^{j,[k+1]} \Delta t}{2} \frac{\partial^2 Ad}{\partial t \partial y}\right)_{i,m,n}^{\langle n+1\rangle,[k]} + \cdots \\
&+ \sum_j \frac{\Delta t}{2\phi_{m,n}^{\langle n+1\rangle,[k+1]}} \left[\left(u_{x,m,n}^{j,[k+1]}\right)^2 \frac{\partial^2 V_{i,m,n}^{j,[k]}}{\partial x^2} + \left(u_{y,m,n}^{j,[k+1]}\right)^2 \frac{\partial^2 V_{i,m,n}^{j,[k]}}{\partial y^2} + 2 u_{x,m,n}^{j,[k+1]} u_{y,m,n}^{j,[k+1]} \frac{\partial^2 V_{i,m,n}^{j,[k]}}{\partial x \partial y}\right]^{\langle n+1\rangle}
\end{aligned} \tag{11}$$

Table 2
General parameters used for the simulations.

Geometrical data of the reservoir					
Length in axis X n_x	500 m 25 blocks	Length in axis Y n_y	500 m 25 blocks	Layer thickness	5 m
Rock properties					
Porosity	0.25	k_{xx}	200 mD	k_{yy}	200 mD
Initial conditions					
S_o	0.70	S_o^r (EOR)	0.35	$S_a^{rH} = S_o^{rH}$	0.15
Simulation data					
Total time	5000 days	Chemical inj. time	200 days	z_{clN}	0.025
Physical data of the phases					
μ^{aH} Water density	1 cP 1020 kg/m^3	μ^{oH} IFT	20 cP 50 mN/m	Oil density	850 kg/m^3

In Eq. (11) the coefficients $\mathcal{C}_{1,2,3}$ are calculated as follows,

$$\begin{aligned}
\mathcal{C}_1 &= \left(\phi_{m,n} + \Delta t\,\frac{\partial\phi}{\partial t} - \frac{u_{tx,m,n}\Delta t}{2\phi_{m,n}}\,\frac{\partial\phi}{\partial x} - \frac{u_{ty,m,n}\Delta t}{2\phi_{m,n}}\,\frac{\partial\phi}{\partial y}\right)^{\langle n+1\rangle,[k+1]} \\
\mathcal{C}_2 &= \left(\frac{\phi_{m,n}}{\Delta t} - \frac{u_{tx,m,n}}{2\phi_{m,n}}\,\frac{\partial\phi}{\partial x} - \frac{u_{ty,m,n}}{2\phi_{m,n}}\,\frac{\partial\phi}{\partial y} + \frac{u_{tx,m,n}\Delta t}{2\phi_{m,n}}\,\frac{\partial^2\phi}{\partial t\partial x} + \frac{u_{ty,m,n}\Delta t}{2\phi_{m,n}}\,\frac{\partial^2\phi}{\partial t\partial y}\right)^{\langle n+1\rangle,[k+1]} \\
\mathcal{C}_3 &= \left(1 - \frac{\Delta t}{2\phi_{m,n}}\,\frac{\partial\phi}{\partial t}\right)^{\langle n+1\rangle,[k+1]}
\end{aligned} \tag{12}$$

2.2.1. Adsorption

The adsorption process occurs when polymer aggregates form onto the surface of the formation rock. This irreversible phenomenon will cause a loss of polymer in the porous media, making the whole process economically unfeasible in case of high rates of adsorption. This is due to the fact that extra chemical would be necessary and the viscosifying properties will be decreased. The adsorption isotherm is rather dependent on the type of polymer, the characteristics of the rock and the type of electrolytes present in the solution. The process starts with aggregates which are formed at the surface. The adsorption of the chemical component onto the rock used in this simulator is described by the Langmuir monolayer model [14,37]:

$$Ad_c = \min\left[\left(Z_c + Ad_c\right), \frac{a_{1,c}\cdot Z_c}{1 + a_{2,c}\cdot Z_c}\right] \tag{13}$$

where a_1 and a_2 are constant parameters based on the salinity and the absolute permeability, and Ad_c is a dimensionless parameter representing the adsorbed volume of chemical component per unit of volume of the porous media. Since it was assumed the fluids are incompressible, adsorption is then formulated on a volume basis.

3. Results and discussion

3.1. Introduction

The polymer flooding will be simulated in an oil field with initial conditions similar to those after the primary recovery (i.e., natural driven mechanisms) was finished. After an initial period with an aqueous polymer solution being injected, a water bank follows in order to drive the polymer slug towards the producing well. For this first stage of simulation, the mechanisms of adsorption, diffusion/dispersion and capillary pressure are neglected and the degradation rate's influence is studied. Subsequently, all the mechanisms will be taken into account to understand their impact in the model. Moreover, different flux-limiting schemes are also evaluated to measure the influence of the numerical diffusion and dispersion in the results.

3.1.1. Data

The physical and operational constraints defined in Tables 2 and 3 are meant to study a polymer EOR flooding and were based on previous studies aimed at representing a standard oilfield with light oil [16].

3.2. Influence of the numerical scheme

Numerical discretization schemes also play an important role in the result of numerical simulations. Mass conservation equations with advective terms are sensitive to the former. [13,35,36,38] A way to diminish the error is to employ higher

Table 3
Physical data and operating conditions of the wells.

Physical data					
Number of wells	2	Well radius	0.25 m	Skin factor	0
Operating conditions					
Total flowrate	1650 STB/day	Bottomhole pressure	55160 kPa		

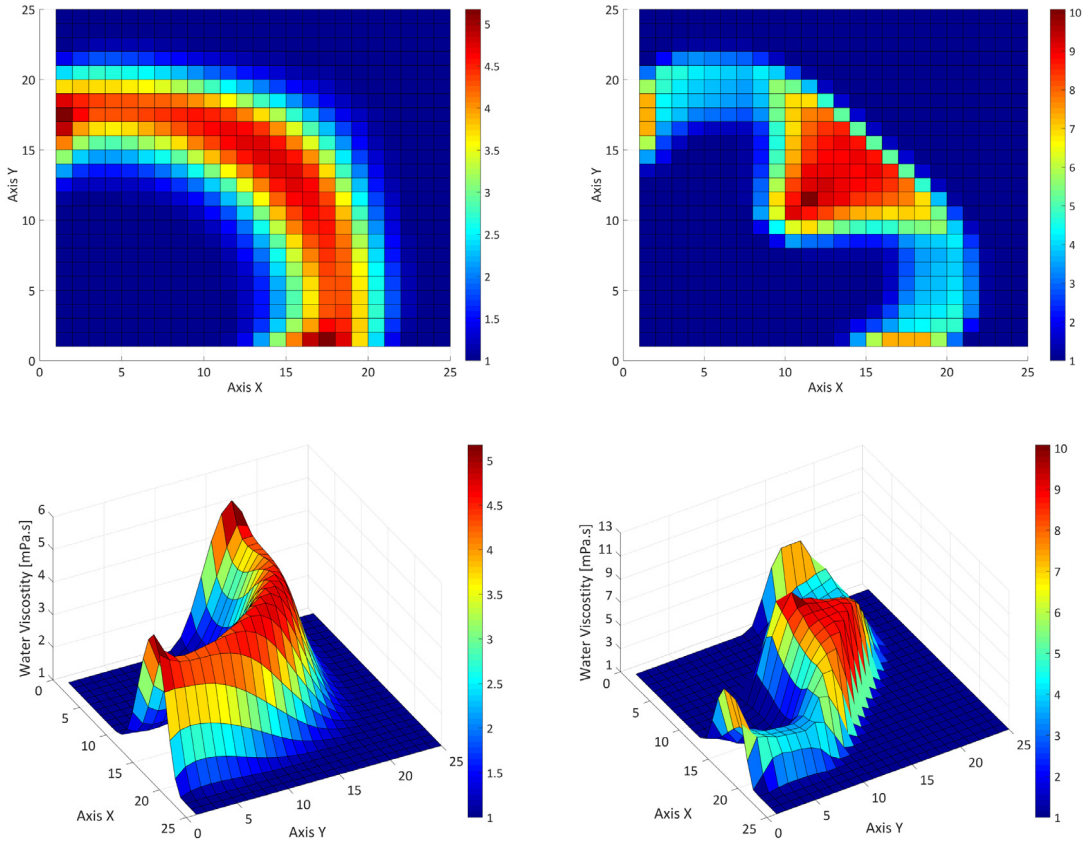

Fig. 3. Aqueous phase viscosity [mPa s] after 1000 days for the upwind (left) and MUSCL (right) schemes.

order numerical schemes, with less numerical diffusion and dispersion. In this simulator flux limiters are used due to a number of advantages, namely: higher-order of accuracy, less diffusion/dispersion and ability to track a steep front-wave. There are several flux limiter formulations, among them: minmod, MUSCL, and superbee. [13,34,39–42] These are a set of piece-wise functions used in numerical methods to solve hyperbolic type partial differential equations, such as the advective mass transport (Eq. (2)). The main objective is to avoid the creation of spurious oscillations that would appear in higher-order discretization schemes when solving the polymer component front tracking. The combined use of determined flux-limiting functions along with high-order discretization schemes renders a Total Variation Diminishing (TVD) solution. TVD schemes allow capturing sharper shocks, reducing numerical diffusion without creating false shock predictions or spurious oscillations which commonly appear in second order accuracy schemes. The simulator was tested under the same physical operating conditions, during an EOR polymer process with degradation, and the results are presented in Figs. 3 to 5.

In the first-order Upwind method, the extra diffusive term causes a flattening and widening of the polymer slug, which ultimately decreases artificially the sweeping efficiency, as shown in Figs. 4 and 5. In the Upwind method the polymer solution front is not clearly determined, but it is shown as a gradual increase in the concentration and a decrease in the oil saturation. The overall simulation behavior is presented in Fig. 6. Flux limiting methods yielded similar results, though a slight difference is appreciated between MinMod and Superbee/MUSCL schemes. Upwind technique rendered a lower recovery factor, as previously indicated in the literature [35]. Fractional flow, oil/water flowrates and pressure drop show that major differences appear only during the chemical breakthrough, when the gradients in concentrations in the producing well reach their maximum values. Regarding the chemical slug, the peak in the four schemes occurs at

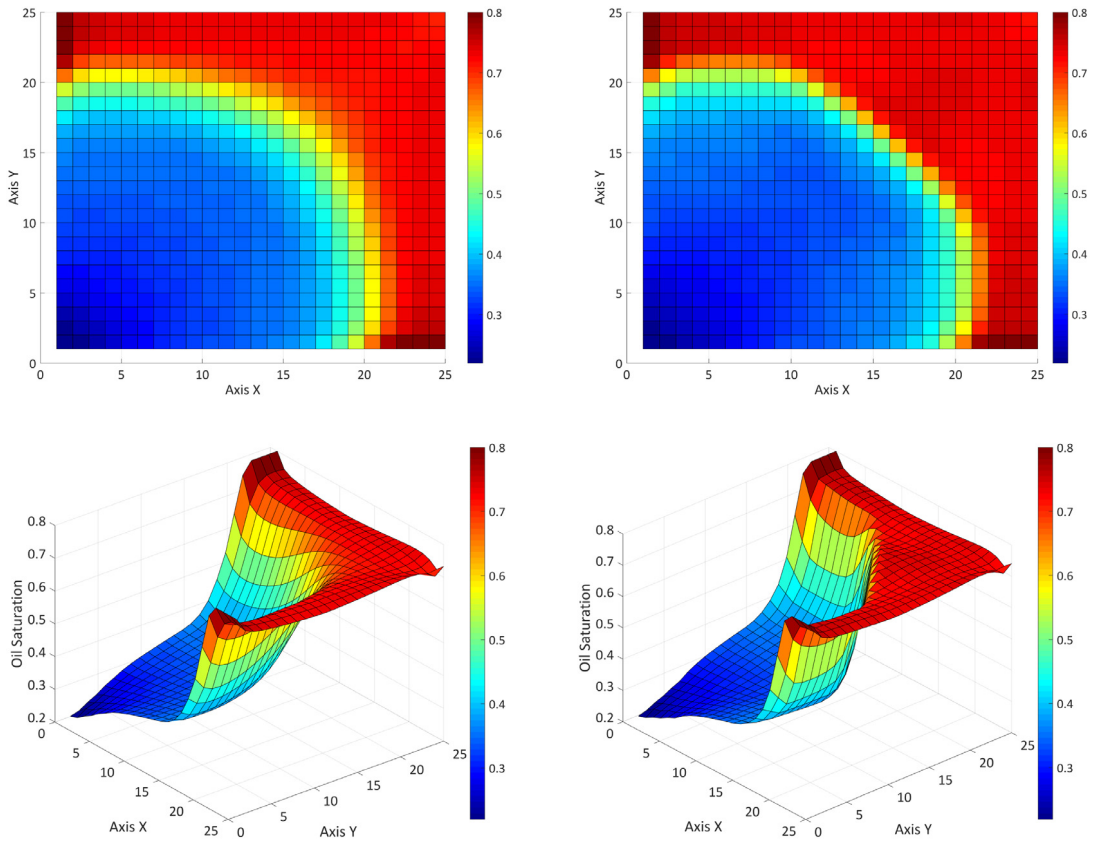

Fig. 4. Oil saturation profiles after 1000 days for the Upwind (left) and MUSCL (right) schemes.

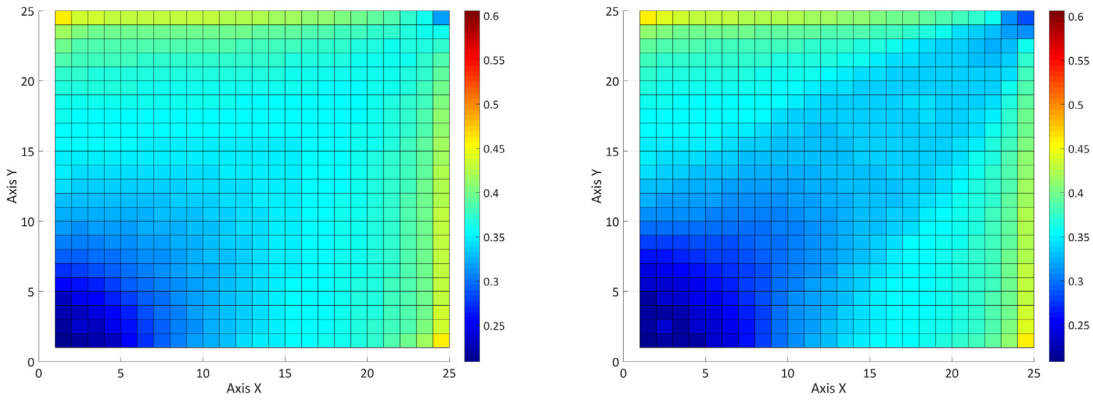

Fig. 5. Final oil saturation profiles after 5000 days for the upwind (left) and MUSCL (right) schemes.

the same time, but with a clear difference between the flux-limiting methods and the Upwind scheme. Due to the extra artificial diffusion, the chemical breakthrough in the upwind method takes place first, followed by MinMod and at last by MUSCL and Superbee techniques. The behavior of the flux limiters also corresponds with results previously reported [36]. These also showed that the splitting technique for flux-limiting problems in 2D systems is a valid approach which can be employed in chemical EOR process in compositional simulation.

3.3. Influence of the chemical adsorption

One of the most relevant problems in CEOR is the adsorption of the chemical species in the porous media. This has a strong negative effect on the recovery factor and sweeping efficiency, since the enhancement of the properties in the

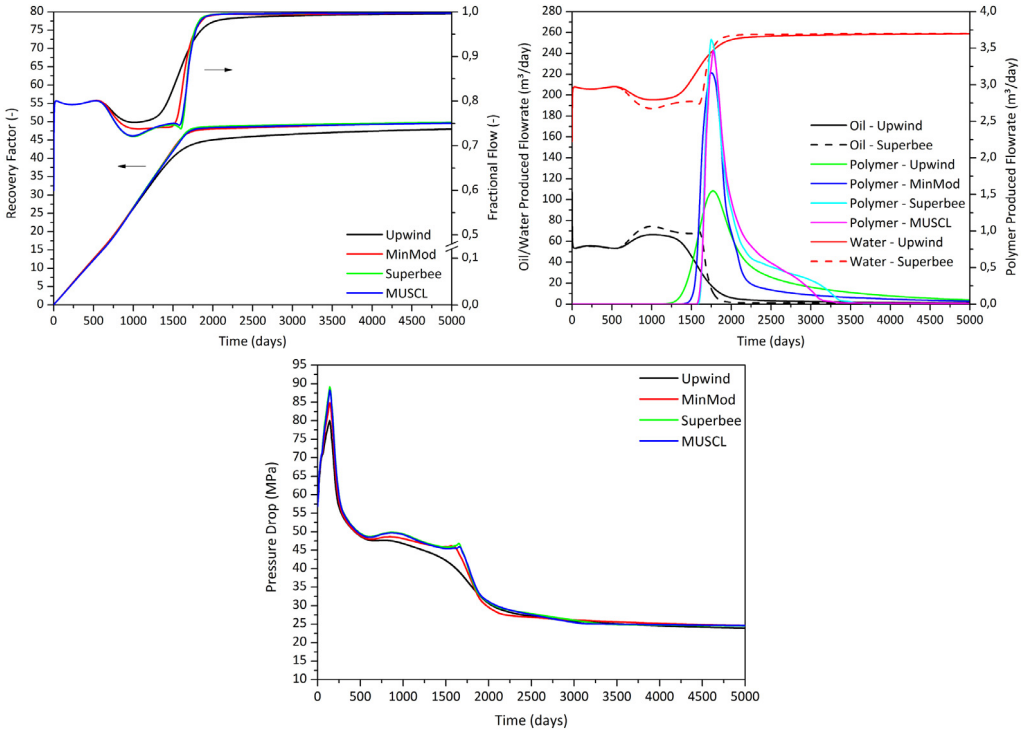

Fig. 6. Cumulative oil production and fractional flow (top left), oleous/aqueous/polymer produced flowrates (top right); and pressure drop (bottom) for the different numerical schemes in a chemical EOR flooding.

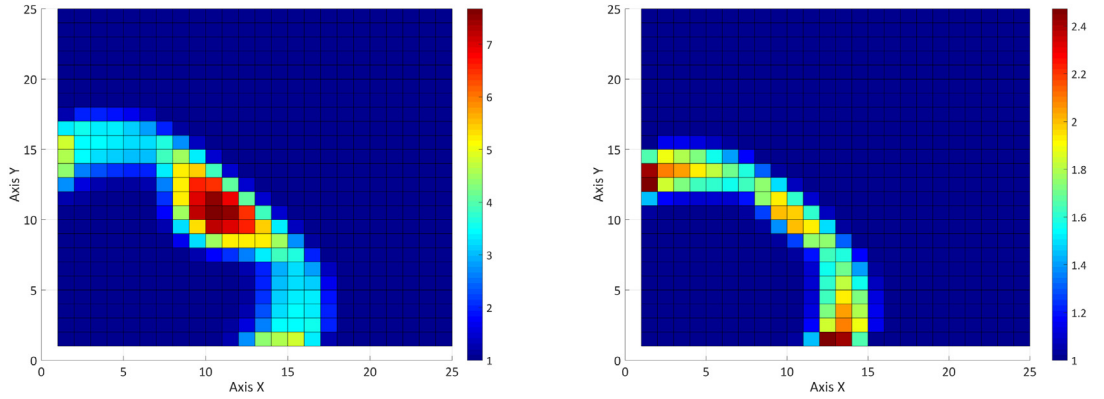

Fig. 7. Aqueous phase viscosity [mPa·s] after 750 days for the linear adsorption with $a_1 = 0.025$ (left) and $a_1 = 0.05$ (right).

aqueous phase is related to the concentration of chemical present. Moreover, since product is being lost in the medium, extra chemical (polymer or surfactant) must be injected in order to counteract the adsorption, increasing the final cost of the process. The amount of mass lost can be calculated thanks to the Langmuir model (Eq. (13)), in which constants a_1 and a_2 are dependent on the salinity present in the system. For the purpose of this model it will be considered a constant salinity content throughout the field.

In order to analyze the influence of the adsorption in the model, several cases will be studied and compared with the base case with no adsorption. The values of the constant a_2^j adopted are linear adsorption, with no limit on the amount of mass adsorbed ($a_2^j = 0$), and Langmuir adsorption ($a_2^j = 3$). These values were adopted from previous chemical simulators [14] and the objective here is to present the influence and trend of this phenomenon in the oil recovery. The analysis of the adsorption constants should be carefully made beforehand in order to assess the future performance of the chemical being injected. The constant a_1 determines the level of adsorption of the chemical species in the medium. The results for the base case and the adsorption cases are shown in Figs. 7 and 8.

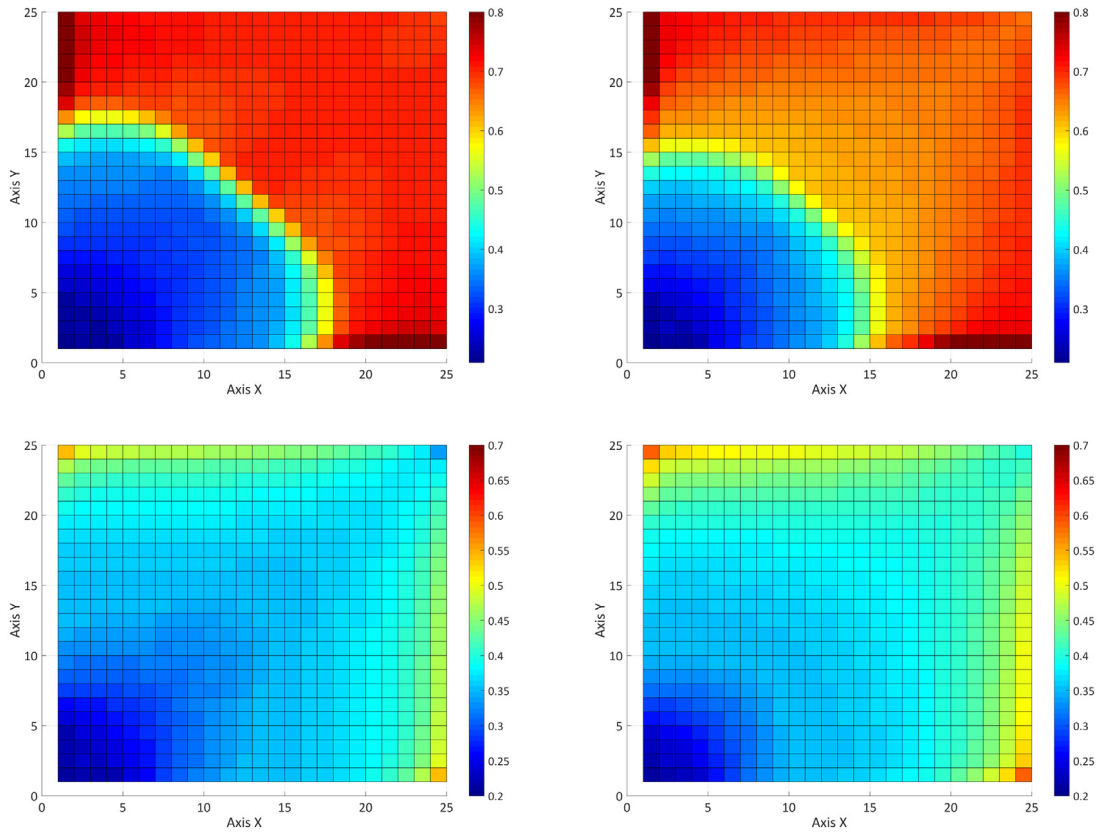

Fig. 8. Oil saturation profiles after 750 (top) and 5000 (bottom) days, for the Langmuir adsorption cases with $a_1 = 0.025$ (left) and $a_1 = 0.05$ (right).

The influence of the adsorption terms becomes evident as the loss of the polymer in the medium causes a steady decrease in the viscosity of the aqueous phase, and therefore in the sweeping efficiency. However, as it is showed in Fig. 8, the behavior at the beginning of the process is similar in both cases, with the same degree of desaturation near the injection well. The difference is thereafter, when the viscosifying properties are lost, and the polymer solution (with $a_1 = 0.025$) achieves a better sweeping efficiency in the corners and near the producing well. Similar trends are observed in Fig. 9 with pressure drop, fractional flow and recovery factor. The former shows a similar response at the beginning, with a pressure peak due to the polymer injection. Nevertheless, in the cases with adsorption these values then decrease and show a curve similar to a waterflooding, but with higher final pressure drop values due to the permeability reduction phenomenon.

When $a_1 = 0.05$ the loss due to adsorption causes the polymer to be adsorbed completely onto the rock and renders the lowest oil recovery factors (Fig. 9), tending to resemble a waterflooding process. A consequence of this process is that the amount of polymer produced is negligible (Fig. 9 — top right). The difference between linear ($a_2 = 0$) and Langmuir ($a_2 = 3$) adsorption models is also noticeable, though the difference is relatively negligible. As it was expected, Langmuir model limits the amount of polymer adsorbed, which ultimately increases the recovery factor, and slightly the pressure drop. Fig. 9 shows also the produced flowrates for each component during the simulation. The most important aspect is that the adsorption delayed the occurrence of the chemical breakthrough, reaching when $a_1 = 0.025$ a peak value one order of magnitude less than cases with no adsorption, and becoming completely negligible when $a_1 = 0.05$.

3.4. Influence of the dispersion

The mass conservation equation is mainly dominated by two driving forces: advective and dispersive. The objective in this section is to present the results when the latter is taken into account and study its consequences. This driving force causes a spreading of the chemical species in the domain, with the immediate consequence of a decrease in the peak concentration, and therefore in the aqueous phase viscosity (Fig. 10). The outcome of this phenomenon is a decrease in the sweeping efficiency since the mobility ratio increases, and the polymer flooding tends to behave like a waterflooding as the process evolves.

The results of four different cases are presented in Figs. 11 and 12. The base case will be the previously studied polymer flooding with degradation and no dispersion. As it was mentioned, the dispersion tensor caused the chemical component

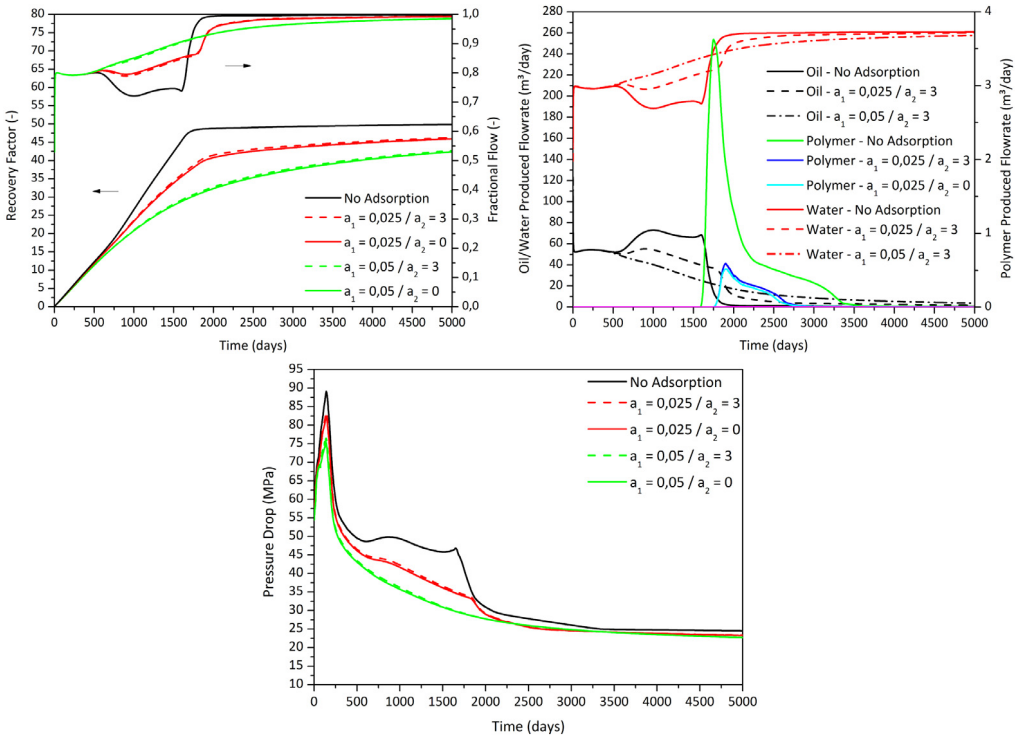

Fig. 9. Cumulative oil production and fractional flow (top left), oleous/aqueous/polymer produced flowrates (top right); and pressure drop (bottom) for a chemical EOR flooding with adsorption.

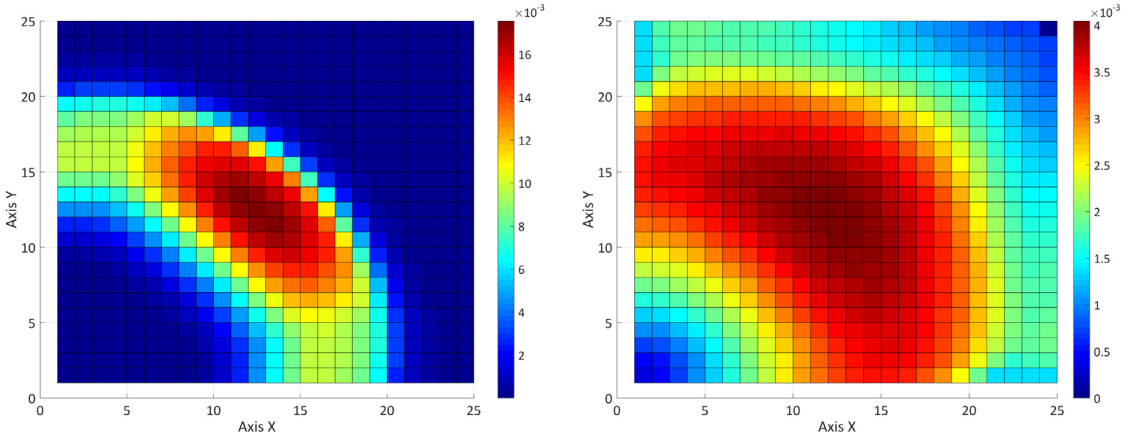

Fig. 10. Polymer concentration after 750 days for the dispersion case with $D_c^a = 5\ \mathrm{m}^2/\mathrm{s}$ (left) and $D_c^a = 50\ \mathrm{m}^2/\mathrm{s}$ (right).

to spread in the domain, lowering its maximum value (Fig. 10). The spreading of the chemical component has a similar behavior as the numerically-introduced diffusion in the upwind method, causing a smearing of the polymer in the porous medium and a decrease in the recovery factor. This is an important reason why diffusive schemes should be avoided when dealing with dispersive processes, since the addition of physical and numerical diffusion phenomena would cause a significant decrease of the oil recovered due to the smearing of the polymer front, reducing the viscosity and therefore increasing the mobility ratio, which affects ultimately the macroscopic sweeping efficiency.

Fig. 10 shows the polymer concentration profile for the extreme dispersive cases studied. When $D_c^a = 5\ \mathrm{m}^2/\mathrm{s}$, the polymer slug still conserves the wave propagating shape, though it is clearly observed that the front wave is not as steep as in the no dispersion case. On the other case, with $D_c^a = 50\ \mathrm{m}^2/\mathrm{s}$ is evident that the polymer slug after 750 days was spread throughout the domain and the concept of polymer slug is no longer valid. Fig. 11 presents the oil saturation profiles after 750 days (top) and at the end of the simulation (bottom). Near the injection well the residual saturation profile is nearly

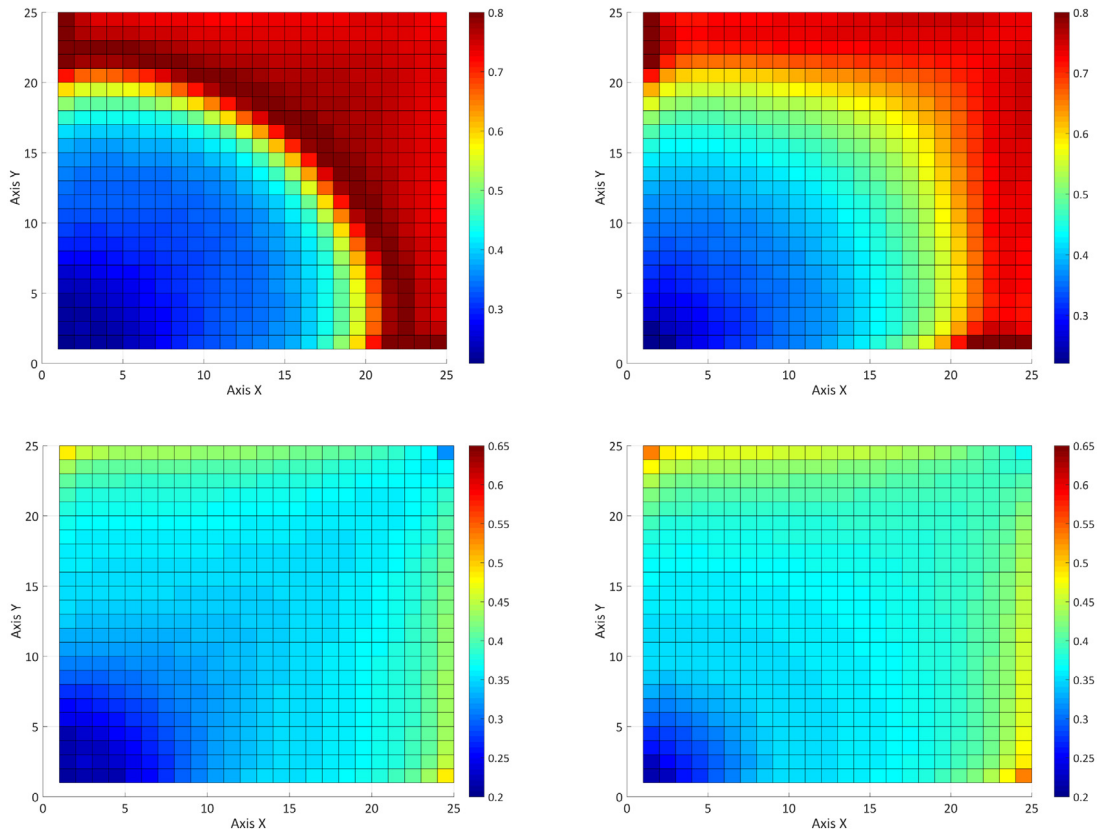

Fig. 11. Oil saturation profiles after 750 (top) and 5000 (bottom) days for the dispersion case with $D_c^a = 5$ m^2/s (left) and $D_c^a = 50$ m^2/s (right).

identical in both cases since there was not enough time for the dispersive forces to decrease the sweeping efficiency of the aqueous solution. However, in the rest of the formation it is evident that diffusive forces caused the polymer concentration to drop to values where the displacing phase could not mobilize the oil towards the producing well.

Fig. 12 presents the general results of the simulation compared to the base case with no dispersion. The recovery factor decreased as the latter increased, though it is clear that at the beginning of the simulation the higher dispersive cases performed better than the no-dispersion case. This is due to the fact that the polymer slug moved faster in the porous media, increasing the recovery at the beginning but yielding lower values at the end because of this phenomenon. This is also appreciated in the fractional flow plot, where minimum values are achieved faster in dispersive cases, but for a shorter period of time. No dispersion case renders higher minimum fractional flows though it remains for a longer period of time, which increases the recovery factor. Pressure drop plot (Fig. 12 — bottom) also shows a clear trend during the simulation. Higher pressure drop peaks are attained in low- and no-dispersive cases, while the maximum peak decreases noticeably in the case with $D_c^a = 50$ m^2/s, since the viscosity of the solution decreases swiftly as the polymer concentration spreads in the rock. The evidence of the faster chemical breakthrough is showed in Fig. 12 (top right). In this case the chemical breakthrough occurs almost immediately, but the maximum flowrate is lower than the no dispersive case, and the broadening of this curve is directly related with these dispersive driving forces.

As a final analysis of the influence of the dispersion tensor in the polymer EOR recovery process, a study is performed considering the joint effect of adsorption and dispersion. In this case only a Langmuir model ($a_2 = 3$) is simulated. Both phenomena were already presented, and the addition of both is expected to lower the results previously obtained. However, it is well known from the literature [2,22,29] that the loss of material because of adsorption is more relevant that the mass transport due to the dispersion tensor. It is because of this reason that the behavior of the system was more sensitive to the adsorption mechanism (Figs. 13 and 14).

Fig. 15 shows the general results of the simulation process. The most relevant result to be noted is the behavior of the chemical slug in the case with $a_1 = 0.025$. In the pure adsorption case, the chemical breakthrough was delayed due to the loss of chemical species in the porous medium. The intensity of the peak is roughly the same obtained previously, but the influence of the dispersion tensor accelerated the breakthrough and made it occur before the base case, but later than the dispersion case only (Figs. 12 and 15). The influence of the dispersion in the recovery factor is showed in Fig. 15. The difference between the two cases ($D_c^a = 5/10$ m^2/s, with $a_1 = 0.05$ and $a_2 = 3$) is negligible, with the less dispersive

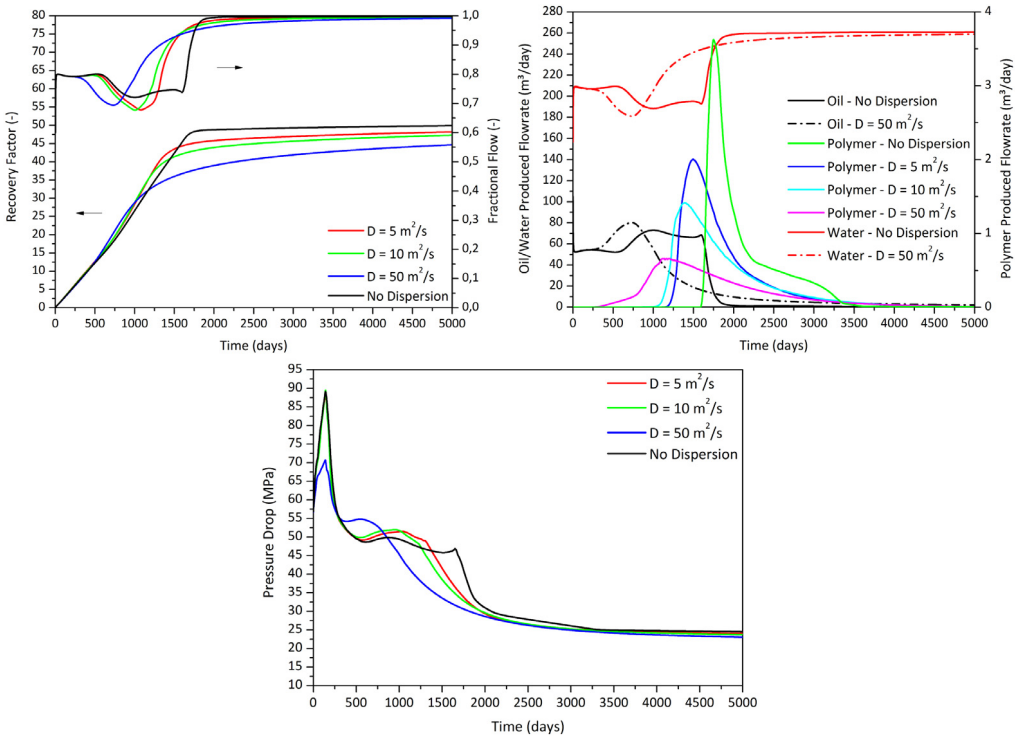

Fig. 12. Cumulative oil production and fractional flow (top left), oleous/aqueous/polymer produced flowrates (top right); and pressure drop (bottom) for a chemical EOR flooding with dispersion.

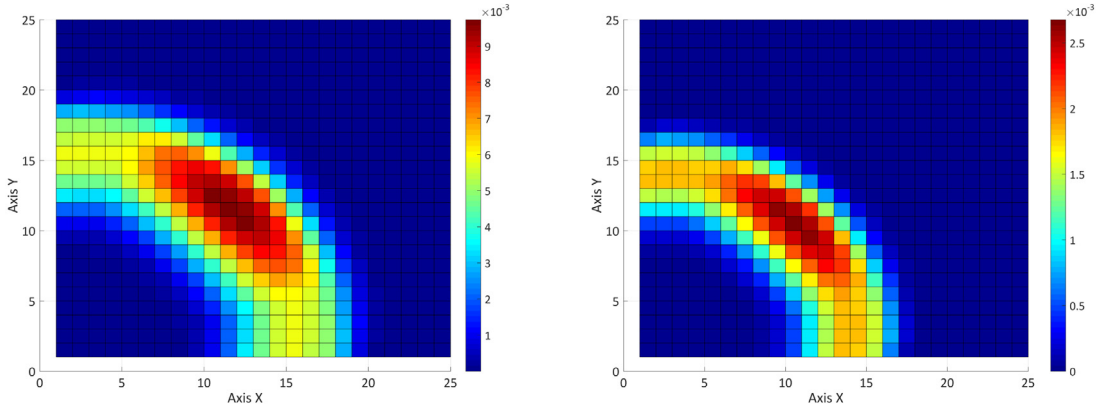

Fig. 13. Polymer concentration after 750 days for the dispersion and adsorption case with $D_c^a = 5\ \mathrm{m}^2/\mathrm{s}$, $a_2 = 3$, and $a_1 = 0.025$ (left) and $a_1 = 0.05$ (right).

case having a recovery factor 0.2% higher. This can be explained due to several factors: the higher dispersion tensor acted spreading the polymer, lowering the viscosity and the sweeping efficiency; but more important, the adsorption effect caused a rapid loss of chemical species. These two factors combined caused that there is only a slight difference between the two models, with the less dispersive recovering more oil.

4. Conclusions

The aim of this paper was to present a study of different physical phenomena taking place in porous media during polymer EOR flooding as well as discussing the influence of the numerical discretization schemes in the recovery efficiency. A new multiphase, multicomponent model was introduced, considering in its development all the important physical parameters present in a chemical flooding and moreover, including a novel mathematical formulations for significant

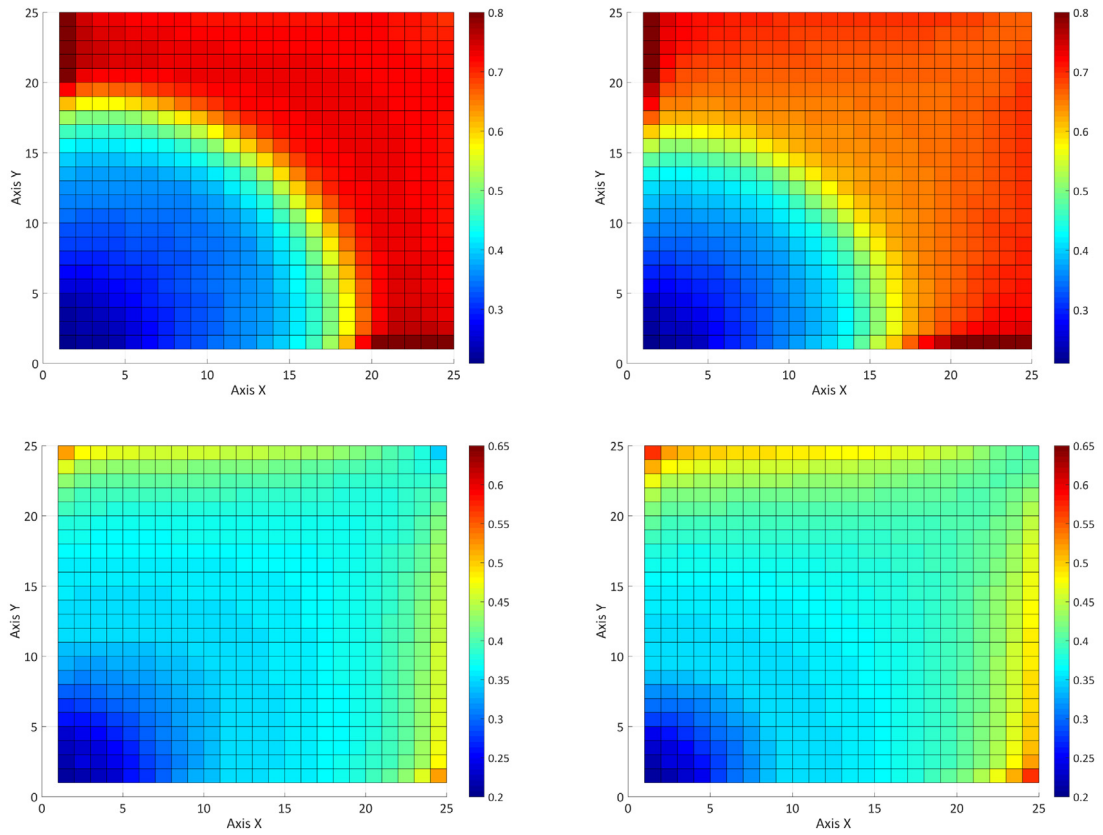

Fig. 14. Oil saturation profiles after 750 (top) and 5000 (bottom) days, for the dispersion and adsorption case with $D_c^a = 5$ m^2/s, $a_2 = 3$, and $a_1 = 0.025$ (left) and $a_1 = 0.05$ (right).

parameters in the process, such as the degradation rate and the polymer viscoelasticity. It is deemed that the use of a simulator which considers all the conditions to which the polymer is submitted is vital for the development and synthesis of new products resistant to the harsh environment present underground. In addition to these phenomena, the numerical scheme developed for this model has the advantage of reducing the numerical round-up errors, as well as present an accurate front-tracking of the polymer slug which, with traditional methods (e.g., Upwind, Lax–Wendroff), it would be impossible, since artificial diffusion and dispersion would affect significantly the results.

The study of the aforementioned properties, along with the physical phenomena modeled and reported in the literature (e.g. rheology, permeability reduction, polymer degradation) is essential to model processes that resemble the results in laboratory and field tests. These show that, of all the presented physical phenomena, adsorption and aqueous phase rheology play a major role in the efficiency of the process. Excessive adsorption rates, along with the degradation of the macromolecules, causes a substantial decrease in the aqueous phase viscosity, hence increases the mobility ratio, provoking the formation of viscous fingering. The dispersion, on the other hand, caused as well a detriment in the efficiency of the process, although its effect was considerably lower than with the adsorption. Finally, it was shown that numerical methods used in the discretization indeed affect the oil recovery in 2D fields. The artificial diffusion caused by the first-order Upwind diminishes the maximum polymer concentration, decreasing slightly the viscosity and affecting negatively the recovery factor. TVD methods, on the other hand, do not suffer the appearance of this artificial diffusion and all the models rendered similar results in terms of oil recovered, with the Superbee being the most accurate one, as reported by several authors. Consequently, a comprehensive study of these phenomena should be mandatory during synthesis and application of new macromolecules for polymer EOR.

Acknowledgments

P.D. gratefully acknowledges the support of the Erasmus Mundus EURICA scholarship program (Program Number 2013-2587/001-001-EMA2) and the Roberto Rocca Education Program, Argentina.

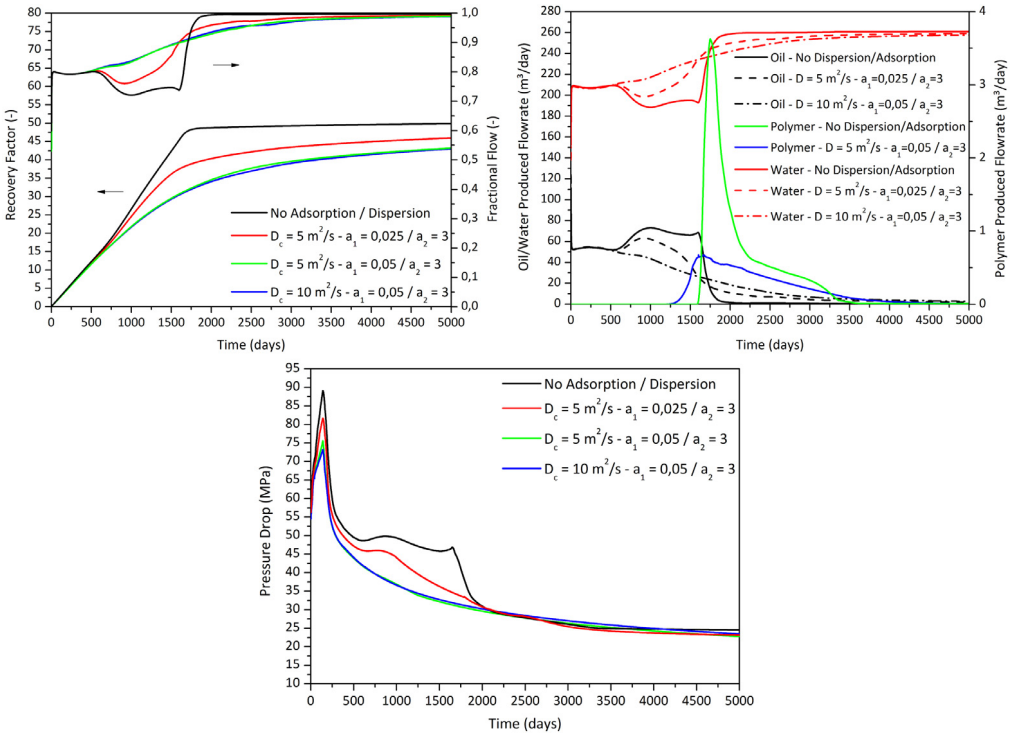

Fig. 15. Cumulative oil production and fractional flow (top left), oleous/aqueous/polymer produced flowrates (top right), and pressure drop (bottom) for a chemical EOR flooding with dispersion.

References

[1] L.P. Dake, Fundamentals of Reservoir Engineering, Elsevier, Amsterdam, the Netherlands, ISBN: 0-444-41830-X, 1978.
[2] L.W. Lake, Enhanced Oil Recovery, Prentice-Hall Inc., Englewood Cliffs, USA, ISBN: 0-13-281601-6, 1989.
[3] T. Sochi, Non-Newtonian flow in porous media, Polymer 51 (22) (2010) 5007–5023, http://dx.doi.org/10.1016/j.polymer.2010.07.047.
[4] T. Sochi, Flow of non-Newtonian fluids in porous media, J. Polym. Sci. Part B 48 (23) (2010) 2437–2467, http://dx.doi.org/10.1002/polb.22144.
[5] H. Zhong, W. Zhang, H. Yin, H. Liu, Study on mechanism of viscoelastic polymer transient flow in porous media, Geofluids (2017) http://dx.doi.org/10.1155/2017/8763951, UNSP 8763951.
[6] R. Cao, L. Cheng, P. Lian, Flow behavior of viscoelastic polymer solution in porous media, J. Dispers. Sci. Technol. 36 (1) (2015) 41–50, http://dx.doi.org/10.1080/01932691.2014.882260.
[7] N. Zamani, R. Kaufmann, P. Kosinski, A. Skauge, Mechanisms of non-Newtonian polymer flow through porous media using Navier–Stokes approach, J. Dispers. Sci. Technol. 36 (3) (2015) 310–325, http://dx.doi.org/10.1080/01932691.2014.896221.
[8] A. Kamyabi, S.A.A. Ramazani, Simulation of two generalised Newtonian fluids flow in micropore with dead end, Int. J. Comput. Fluid Dyn. 25 (3) (2011) 163–173, http://dx.doi.org/10.1080/10618562.2011.575370.
[9] A. Kamyabi, A. Ramazani, M.M. Kamyabi, Effects of viscoelastic polymer solutions on the oil extraction from dead ends, Sci. Iran. 20 (6) (2013) 1912–1920.
[10] Z. Zhang, J. Li, J. Zhou, Microscopic roles of "viscoelasticity" in HPMA polymer flooding for EOR, Transp. Porous Media 86 (1) (2011) 229–244, http://dx.doi.org/10.1007/s11242-010-9616-6.
[11] M. Delshad, D.H. Kim, O.A. Magbagbeola, C. Huh, G.A. Pope, F. Tarahhom, Mechanistic Interpretation and Utilization of Viscoelastic Behavior of Polymer Solutions for Improved Polymer-Flood Efficiency, 2008, http://dx.doi.org/10.2118/113620-MS.
[12] J. Wang, H.-Q. Liu, J. Xu, Mechanistic simulation studies on viscous-elastic polymer flooding in petroleum reservoirs, J. Dispers. Sci. Technol. 34 (3) (2013) 417–426, http://dx.doi.org/10.1080/01932691.2012.660780.
[13] P. Druetta, P. Tesi, C.D. Persis, F. Picchioni, Methods in oil recovery processes and reservoir simulation, Adv. Chem. Eng. Sci. 6 (04) (2016) 39.
[14] M.S. Bidner, G.B. Savioli, On the numerical modeling for surfactant flooding of oil reservoirs, Mec. Comput. XXI (2002) 566–585.
[15] D.W. Green, G.P. Willhite, Enhanced Oil Recovery, Society of Petroleum Engineers, Richardson, USA, ISBN: 978-1-55563-077-5, 1998.
[16] P. Druetta, J. Yue, P. Tesi, C.D. Persis, F. Picchioni, Numerical modeling of a compositional flow for chemical EOR and its stability analysis, Appl. Math. Model. 47 (2017) 141–159, http://dx.doi.org/10.1016/j.apm.2017.03.017.
[17] J. Bear, Dynamics of Fluids in Porous Media, v. 1, American Elsevier Publishing Company, ISBN: 978-0-44400-114-6, 1972.
[18] Z. Chen, G. Huan, Y. Ma, Computational Methods for Multiphase Flows in Porous Media, Society for Industrial and Applied Mathematics, ISBN: 978-0-89871-606-1, 2006, http://dx.doi.org/10.1137/1.9780898718942.
[19] D. Kuzmin, A Guide to Numerical Methods for Transport Equations, University Erlangen–Nuremberg, Germany, 2010.
[20] N.F. Najafabadi, Modeling Chemical EOR Processes using IMPEC and Fully IMPLICIT Reservoir Simulators (Doctoral dissertation), The University of Texas at Austin, USA, 2009.
[21] P. Druetta, F. Picchioni, Numerical modeling and validation of a novel 2D compositional flooding simulator using a second-order TVD scheme, Energies 11 (2018) 2280, http://dx.doi.org/10.3390/en11092280.
[22] J. Sheng, Modern Chemical Enhanced Oil Recovery, Elsevier, Amsterdam, the Netherlands, ISBN: 978-0-08096-163-7, 2011, 0080961630.

[23] Z. Lijuan, Y. Xiang'an, G. Fenqiao, Micro-mechanisms of residual oil mobilization by viscoelastic fluids, Pet. Sci. 5 (1) (2008) 56–61, http://dx.doi.org/10.1007/s12182-008-0009-1.
[24] R.S. Seright, How much polymer should be injected during a polymer flood? Review of previous and current practices, SPE J. 22 (1) (2017) 1–18, http://dx.doi.org/10.2118/179543-PA.
[25] R.S. Seright, M. Seheult, T. Talashek, Injectivity characteristics of EOR polymers, SPE Reserv. Eval. Eng. 12 (5) (2009) 783–792.
[26] E. Ahusborde, M.E. Ossmani, A Sequential Approach for Numerical Simulation of Two-Phase Multicomponent Flow with Reactive Transport in Porous Media, 2017, http://dx.doi.org/10.1016/j.matcom.2016.11.007.
[27] J. Bear, Y. Bachmat, Macroscopic modeling of transport phenomena in porous-media. 2. Applications to mass, momentum and energy-transport, Transp. Porous Media 1 (3) (1986) 241–269, http://dx.doi.org/10.1007/BF00238182.
[28] B. Braconnier, C. Preux, E. Flauraud, Q.-H. Tran, C. Berthon, An analysis of physical models and numerical schemes for polymer flooding simulations, Comput. Geosci. 21 (5–6) (2017) 1267–1279, http://dx.doi.org/10.1007/s10596-017-9637-0.
[29] D. Camilleri, S. Engelson, L.W. Lake, E.C. Lin, T. Ohnos, G. Pope, K. Sepehrnoori, Description of an improved compositional micellar/polymer simulator, SPE Reserv. Eng. 2 (1987) 427–432, http://dx.doi.org/10.2118/13967-PA.
[30] D. Camilleri, A. Fil, G.A. Pope, B.A. Rouse, K. Sepehrnoori, Comparison of an improved compositional micellar/polymer simulator with laboratory corefloods, SPE Reserv. Eng. 2 (1987) 441–451, http://dx.doi.org/10.2118/12083-PA.
[31] S.T. Hilden, O. Moyner, K.-A. Lie, K. Bao, Multiscale simulation of polymer flooding with shear effects, Transp. Porous Media 113 (1) (2016) 111–135, http://dx.doi.org/10.1007/s11242-016-0682-2.
[32] A. Lohne, O. Nodland, A. Stavland, A. Hiorth, A model for non-Newtonian flow in porous media at different flow regimes, Comput. Geosci. 21 (5–6) (2017) 1289–1312, http://dx.doi.org/10.1007/s10596-017-9692-6.
[33] D.W. Peaceman, Interpretation of well-block pressures in numerical reservoir simulation (includes associated paper 6988), Soc. Pet. Eng. J. 18 (1978) 183–194, http://dx.doi.org/10.2118/6893-PA.
[34] N. Saad, G.A. Pope, K. Sepehrnoorl, Application of Higher-Order Methods in Compositional Simulation, in: SPE Reservoir Engineering, vol. 5, Society of Petroleum Engineers, 1990, pp. 623–630.
[35] K. Kamalyar, R. Kharrat, M. Nikbakht, Numerical aspects of the convection-dispersion equation, Pet. Sci. Technol. 32 (14) (2014) 1729–1762, http://dx.doi.org/10.1080/10916466.2010.490802.
[36] J. Liu, M. Delshad, G.A. Pope, K. Sepehrnoori, Application of higher-order flux-limited methods in compositional simulation, Transp. Porous Media 16 (1) (1994) 1–29, http://dx.doi.org/10.1007/BF01059774.
[37] M. Delshad, G. Pope, K. Sepehrnoori, UTCHEM version 9.0 Technical Documentation, Center for Petroleum and Geosystems Engineering, The University of Texas at Austin, USA 78751.
[38] R. Fazio, A. Jannelli, Second order positive schemes by means of flux limiters for the advection equation, IAENG Int. J. Appl. Math. 39 (1) (2009) 1–11.
[39] D. Kuzmin, S. Turek, High-resolution FEM-TVD schemes based on a fully multidimensional flux limiter, J. Comput. Phys. 198 (1) (2004) 131–158, http://dx.doi.org/10.1016/j.jcp.2004.01.015.
[40] J. Lai, G. Lin, W. Guo, An upstream flux-splitting finite-volume scheme for 2D shallow water equations, Internat. J. Numer. Methods Fluids 48 (10) (2005) 1149–1174, http://dx.doi.org/10.1002/fld.974.
[41] T.S. Mykkeltvedt, X. Raynaud, K.-A. Lie, Fully implicit higher-order schemes applied to polymer flooding, Comput. Geosci. 21 (5–6) (2017) 1245–1266, http://dx.doi.org/10.1007/s10596-017-9676-6.
[42] H. Smaoui, L. Zouhri, A. Ouahsine, Flux-limiting techniques for simulation of pollutant transport in porous media: Application to groundwater management, Math. Comput. Modelling 47 (1–2) (2008) 47–59, http://dx.doi.org/10.1016/j.mcm.2007.02.006.